Density distributions, form factors and reaction cross sections for exotic ^{11}Be and ^{15}C nuclei

Adel K. Hamoudi, Gaith N. Flaiyh, Ahmed N. Abdullah

Department of Physics, College of Science, University of Baghdad, Baghdad, Iraq

E-mail: Ahmednajim1979@yahoo.com

Abstract

The ground state proton, neutron and matter densities of exotic ^{11}Be and ^{15}C nuclei are studied by means of the TFSM and BCM. In TFSM, the calculations are based on using different model spaces for the core and the valence (halo) neutron. Besides single particle harmonic oscillator wave functions are employed with two different size parameters β_c and β_v. In BCM, the halo nucleus is considered as a composite projectile consisting of core and valence clusters bounded in a state of relative motion. The internal densities of the clusters are described by single particle Gaussian wave functions.

Elastic electron scattering proton form factors for these exotic nuclei are analyzed via the plane wave born approximation (PWBA). As the calculations in the BCM do not distinguish between protons and neutrons, the calculations of the proton form factors are restricted only by the TFSM.

The reaction cross sections for these exotic nuclei are studied by means of the Glauber model with an optical limit approximation using the ground state densities of the projectile and target, where these densities are described by single Gaussian functions. The calculated reaction cross sections at high energy are in agreement with the experimental data.

Key words

Halo Nuclei, neutron-rich nuclei, Two-frequency shell model, nuclear density distribution.

Article info.

Received: Mar. 2014
Accepted: May. 2014
Published: Sep. 2014

توزيعات الكثافة, عوامل التشكل والمقاطع العرضية للتفاعل للنوى الغريبة ^{11}Be و ^{15}C

عادل خلف حمودي، غيث نعمة فليح, احمد نجم عبدالله

قسم الفيزياء، كلية العلوم، جامعة بغداد، بغداد، العراق

الخلاصة

تم حساب توزيعات الكثافة البروتونية والنيوترونية داخل النواة بالاضافة الى الكتلية للنوى الهالة الغنية بالنيوترونات ^{11}Be و ^{15}C باستخدام أنموذج القشرة ذو الترددين والأنموذج العنقودي الثنائي. في أنموذج القشرة ذو الترددين استندت الحسابات على استخدام فضاء لنيوكلونات القلب مختلف عما هو عليه لنيوكلونات الهالة. استُخدمت الدوال الموجية للجسيمة المفردة لجهد المتذبذب التوافقي مع قيمتين مختلفتين للثابت التوافقي واحدة للقلب (β_c) و الاخرى للهالة (β_v). في الأنموذج العنقودي الثنائي تم افتراض ان نواة الهالة عبارة عن قذيفة مركبة تتكون من عنقودين هما القلب والهالة تتحركان سوياً بحركة نسبية بالنسبة لمركز كتلتيهما. لقد تم استخدام دالة گاوس للجسيمة المفردة في وصف حركة كل من عنقودي القلب والهالة. لقد تم تحليل نتائج عوامل التشكل المرنة لبروتونات هذه النوى بواسطة تقريب بورن للموجة المستوية. نظراً لكون الحسابات في الأنموذج العنقودي الثنائي لايميز بين البروتونات والنيوترونات لذلك فان حسابات عوامل التشكل اقتصرت فقط على أنموذج القشرة ذو الترددين.

المقاطع العرضية للتفاعل لهذه النوى عند الطاقات العالية تم دراستها باستخدام نموذج گلوبر باستخدام توزيع الكثافة للحالة الارضية للنواة القذيفة والهدف، حيث ان هذه الكثافات توصف بواسطة دوال گاوس للجسيمة المنفردة. ان حسابات المقاطع العرضية للتفاعل تتفق بشكل جيد مع القيم العملية.

Introduction

Since the discoveries of neutron halo in exotic light neutron-rich nuclei in the mid-eighties [1,2], studies on halo phenomena have become a hot point in nuclear physics. The cause of halo phenomena lies in both the small separation energy of the last few nucleons and their occupation on the orbits with low angular momentum (l = 0, 1) [3], which allow the wave function of the valence nucleons to extend to large radii [4]. The observation of large total interaction cross sections for ^{11}Li, ^{11}Be, and ^{14}Be was done by Tanihata *et al*. [1] showed that halo is probably present in many neutron-rich nuclei close to the drip line and initialized intensive experimental and theoretical work on neutron-rich nuclei. Such a behavior shows up also on the proton-rich side of the chart of nuclei [4]. But the study of proton-rich nuclei is scarce as compared with that of neutron-rich nuclei. It is believed that it is slightly hard for proton-rich nuclei to form the halo structure because of Coulomb barrier [5], which hinder the proton to penetrate into the out region of the nuclear-core [6].

The halo nuclei have large neutron excess or proton excess where a few outside nucleons are very weakly bound. Such halo systems are well described by the few body models, which assume that halo nuclei consist of a tightly bound inner core surrounded by a few outer nucleons that are loosely bound to it [7]. So the halo nuclei can be divided into two types : the two-body halo where one nucleon is surrounding the core nucleus, such as the one-neutron halo ^{11}Be and the one-proton halo ^{8}B; and the three-body halo where two valence nucleons are around the core nucleus, such as ^{6}He and ^{11}Li [8]. The three-body halo have been called Borromean because where the two-body subsystems (core plus one neutron or the di-neutron) are unbound, but the three-body system is bound [9, 10].

The halo nuclei are so short lived that they cannot be used as targets at rest. Instead, direct reactions with radioactive nuclear beam (RNB) can be done in inverse kinematics, where the role of beam and target are interchanged [11].

The electron scattering from nuclei is a powerful to investigate the electromagnetic structure in stable nuclei. This is because of the relatively weak interaction of electron with nucleus which is done through the well-known electromagnetic force. Electron scattering from exotic nuclei is not presently available; the technical proposal for the construction of electron-ion collider at GSI/Germany[12] and RIKEN/Japan facility [13] will be a great opportunity to study the electromagnetic structure of these exotic nuclei in the near future.

Many theoretical and experimental studies [14-20] have discussed and confirmed the halo structure in ^{11}Be and ^{15}C exotic nuclei.

The total nuclear reaction cross section (σ_R) is one of the most important physical quantities characterizing the properties of nuclear reaction [21]. It is very useful for extracting fundamental information about the nuclear size and the density distributions of neutrons and protons in nucleus. In particular, the neutron halo has been found by measuring the total reaction cross section induced by radioactive nuclear beams [1, 22]. The definition of the reaction cross section (σ_R) and the interaction cross section (σ_I) are as follows [23]:

$$\sigma_R = \sigma_{tot} - \sigma_{ela}$$

$$\sigma_I = \sigma_R - \sigma_{inela}$$

where σ_{tot}, σ_{ela} and σ_{inela} are the total reaction cross section, the elastic scattering cross section, and the inelastic scattering cross section, respectively. The reaction cross section (σ_R) can be described by subtracting the σ_{ela} from the σ_{tot}. The

interaction cross section (σ_I) is the probability of the reaction which the proton number and/or the neutron number of the projectile particle are changed. The inelastic scattering cross section is the probability of the reaction in which a projectile nucleus and/or a target nucleus is excited due to the collision. At high energy (above several hundred MeV/nucleon), it is known that the σ_R is approximated by σ_I $(\sigma_R \approx \sigma_I)$ because the contribution of the inelastic scattering is low [24, 25].

One of the widely used models for analyzing the interaction and the reaction cross sections of nucleus-nucleus scattering is the Glauber model [26]. A simple Glauber model has had to be used to connect the density distributions and cross sections. Although the model is simple, it shows reasonable results for many cases [27]. For the reactions of the stable and exotic nuclei, agreements have been obtained between calculation and experimental value for reaction cross section by using the simplified Glauber models at the incident energy around GeV/nucleon. A modified microscopic Glauber theory was presented in Refs. [26, 28] in order to investigate the reaction projectile-target collisions at low and intermediate energies. The calculations of reaction cross section by using modified microscopic Glauber theory at intermediate energies are in good agreement with the experimental data, but it can only be used to investigate the halo nucleus.

Theory

The one-body operator of the longitudinal transition density for point protons (with isospin $t_z = 1/2$) or neutrons ($t_z = -1/2$) is given by [29]

$$\hat{\rho}^{L}_{\Delta J,t_z} = \sum_{k=1}^{A} e(t_z) \frac{\delta(r - r_k)}{r_k^2} Y_{\Delta J, M_{\Delta J}}(\Omega_{r_k}), \quad (1)$$

with

$$e(t_z) = \frac{1 + 2t_z(k)}{2}.$$

In Eq. (1), the superscript (L) in the operator $\hat{\rho}^{L}_{\Delta J,t_z}$ stands for a longitudinal operator, $Y_{\Delta J, M_{\Delta J}}(\Omega_{r_k})$ and $\delta(\vec{r} - \vec{r}_k)$ are the spherical harmonic and Dirac delta functions, respectively. The multipolarity ΔJ of the transition is restricted by the following angular momentum and parity selection rules:

$$\left| J_i \_ J_f \right| \le \Delta J \le J_i + J_f$$

and

$\pi_i \pi_f = (-1)^{\Delta J}$ (for Coulomb transitions).

The reduced matrix element of Eq. (1) is expressed as [29]

$$\left\langle J_f \left\| \hat{\rho}^{L}_{\Delta J,t_z}(\vec{r}) \right\| J_i \right\rangle = \frac{1}{\sqrt{4\pi(2J_i + 1)}} \sum_{ab} OBDM(J_f, J_i, \Delta J, a, b, t_z) \left\langle j_a \left\| Y_{\Delta J} \right\| j_b \right\rangle R_{n_a l_a}(r) R_{n_b l_b}(r), \quad (2)$$

where a and b label single-particle states for the considered shell model space, i.e. $|a\rangle = |n_a l_a\rangle |j_a m_a\rangle$ and $|b\rangle = |n_b l_b\rangle |j_b m_b\rangle$, the states $|J_i\rangle$ and $|J_f\rangle$ are characterized by the model space wave functions, $R_{n_p l_p}(r)$ is the radial part of the harmonic oscillator wave function, $\left\langle j_a \left\| Y_{\Delta J} \right\| j_b \right\rangle$ is the reduced matrix element of the spherical harmonic, $OBDM(J_f, J_i, \Delta J, a, b, t_z)$ is the proton $(t_z = 1/2)$ or neutron $(t_z = -1/2)$ one body density matrix element given by the second quantization as [29]

$$OBDM(J_f, J_i, \Delta J, a, b, t_z) = \frac{\left\langle J_f \left\| \left[a^+_{a,t_z} \otimes \tilde{a}_{b,t_z} \right]^{\Delta J} \right\| J_i \right\rangle}{\sqrt{2\Delta J + 1}}. \quad (3)$$

As the model space wave functions have good isospin, it is appropriate to evaluate the *OBDM* elements by means of isospin-reduced matrix elements. The relation between these triply reduced *OBDM* and the proton or neutron *OBDM* of Eq. (2) is given by [29]

$$OBDM(t_z) = (-1)^{T_f - T_z} \sqrt{2} \begin{pmatrix} T_f & 0 & T_i \\ -T_z & 0 & T_z \end{pmatrix} OBDM(\Delta T = 0)/2 \quad (4)$$
$$+ 2t_z (-1)^{T_f - T_z} \sqrt{6} \begin{pmatrix} T_f & 1 & T_i \\ -T_z & 0 & T_z \end{pmatrix} OBDM(\Delta T = 1)/2$$

where the triply reduced $OBDM(\Delta T)$ elements are given in terms of the second quantization as

$$OBDM(i, f, \Delta J, \alpha, \beta, \Delta T) = \frac{\left\langle \Gamma_f \left\| \left[a^+_\alpha \otimes \tilde{a}_\beta \right]^{\Delta J, \Delta T} \right\| \Gamma_i \right\rangle}{\sqrt{2\Delta J + 1}\sqrt{2\Delta T + 1}} \quad (5)$$

Here, Greek symbols are utilized to indicate quantum numbers in coordinate space and isospace (i.e., $\alpha \equiv a t_a$, $\beta \equiv b t_b$, $\Gamma_i \equiv J_i T_i$ and $\Gamma_f \equiv J_f T_f$).

The $OBDM(\Delta T)$ elements contain all of the information about transitions of given multipolarities which are embedded in the model space wave functions. To obtain these *OBDM* elements, we perform shell model calculations by OXBASH code [30] using realistic effective interactions.

For the ground state density distribution, we have $n_a = n_b$, $l_a = l_b$, $j_a = j_b$, $J_i = J_f$ and $\Delta J = 0$, then Eq. (2) becomes as

$$\rho_{t_z}(r) \equiv \left\langle J_i \left\| \hat{\rho}^L_{\Delta J=0, t_z}(\vec{r}) \right\| J_i \right\rangle \quad (6)$$
$$= \frac{1}{\sqrt{4\pi(2J_i + 1)}} \sum_{ab} OBDM(J_i, J_i, 0, a, b, t_z) \left\langle j_a \| Y_0 \| j_b \right\rangle R_{n_a l_a}(r) R_{n_b l_b}(r),$$

where

$$\left\langle j_a \| Y_0 \| j_b \right\rangle = \left\langle j_a \left\| \frac{1}{\sqrt{4\pi}} \right\| j_b \right\rangle = \frac{1}{\sqrt{4\pi}} \left\langle j_a \| 1 \| j_b \right\rangle = \frac{1}{\sqrt{4\pi}} \sqrt{2j_a + 1}\, \delta_{j_a j_b}. \quad (7)$$

The average occupation number in each orbit n_{a,t_z} is given by

$$n_{a,t_z} = \sqrt{\frac{2J_a + 1}{2J_i + 1}}\, OBDM(J_i, J_i, 0, a, a, t_z). \quad (8)$$

Two approaches are utilized for calculating the ground state densities of exotic halo nuclei considered in the present study, these are (the two frequency shell model and the binary cluster model) outlined in subsections 1 and 2.

1. The two frequency shell model (TFSM)

As the exotic halo nuclei are oversized and easily broken systems consisting of a compact core plus a number of outer nucleons loosely bound and spatially extended far from the core, it is suitable to separate the ground state matter density distribution $\rho_{t_z,m}(r)$ into two parts. The first part is connected to the core nucleons $\rho_{t_z,c}(r)$ while the second is connected to the valence (halo) nucleons $\rho_{t_z,v}(r)$, (for simplicity, the subscript t_z in these densities will be dropped), i.e.

$$\rho_m(r) = \rho_c(r) + \rho_v(r). \quad (9)$$

In TFSM [31,32], the harmonic oscillator wave functions (HO) are used with two different oscillator size parameters β_c (for core nucleons) and β_v (for halo nucleons). This approach permits to work freely on each part by changing $\beta_{c(v)}$ till obtaining a fit with experimental data. Furthermore, the matter density of Eq. (9) may also be expressed as

$$\rho_m(r) = \rho^p(r) + \rho^n(r), \quad (10)$$

where $\rho^p(r)$ and $\rho^n(r)$ are the ground state proton and neutron densities of halo nuclei expressed as

$$\rho^p(r) = \rho^p_c(r) + \rho^p_v(r) \quad (11)$$

and

$$\rho^n(r) = \rho^n_c(r) + \rho^n_v(r). \quad (12)$$

The normalization conditions for the ground state densities given in Eqs. (9-12) are

$$g = 4\pi \int_0^\infty \rho_g(r) r^2 dr, \quad (13)$$

and the corresponding rms radii are

$$< r^2 >_g^{1/2} = \frac{4\pi}{g} \int_0^\infty \rho_g(r) r^4 dr, \quad (14)$$

where $\rho_g(r)$ corresponds to the one of the densities [$\rho_m(r)$, $\rho_c(r)$, $\rho_v(r)$, $\rho^p(r)$, $\rho^n(r)$] and g corresponds to the number of nucleon in each case.

Next we use the plane wave Born approximation (PWBA) to study the elastic electron scattering form factors from considered nuclei. In the PWBA, the incident and scattered electron waves are represented by plane waves. The elastic proton form factor is simply given by the Fourier-Bessel transform of the ground state proton density distribution obtained by TFSM, i.e.

$$F(q) = \frac{4\pi}{Z} \int_0^\infty \rho^p(r) j_0(qr) r^2 dr, \quad (15)$$

where $j_0(qr)$ is the spherical Bessel function of order zero and q is the momentum transfer from the incident electron to the target nucleus. Inclusion the corrections of the finite nucleon size $F_{fs}(q) = \exp(-0.43q^2/4)$ and the center of mass $F_{cm}(q) = \exp(b^2 q^2/4A)$ in the calculations needs multiplying the form factor of Eq. (15) by these corrections.

In the limit $q \to 0$, the target nucleus will be characterized as a point particle. Accordingly, using Eq. (13) with the help of Eq. (9), the proton form factor of the target nucleus will be equal to unity (i.e. $F(q \to 0) = 1$).

2. The binary cluster model (BCM)

In BCM [33], the exotic halo nuclei are considered as composite projectiles of mass A_p and described, in Fig. 1, as core and valence clusters, of masses A_c and A_v bounded with a state of relative motion. It is assumed that $A_c \geq A_v$. For simplicity, the internal densities of the clusters are described by single Gaussian functions with ranges α_c and α_v,

$$\begin{aligned} \rho_c(r) &= A_c g^{(3)}(\alpha_c, r), \\ \rho_v(r) &= A_v g^{(3)}(\alpha_v, r), \end{aligned} \quad (16)$$

where $g^{(3)}$ is the normalized 3-dimensional Gaussian function

$$g^{(3)}(\alpha_{c(v)}, r) = \frac{1}{\pi^{3/2} \alpha_{c(v)}^3} \exp(-r^2/\alpha_{c(v)}^2), \ \int g^{(3)}(\alpha_{c(v)}, r) d\vec{r} = 1, \ < r^2 >_{c(v} = 3\alpha_{c(v)}^2/2. \quad (17)$$

Upon convoluting the intrinsic cluster densities with their center of mass (c.m.) motions about the c.m. of the projectile, the composite projectile density is given by [33]

$$\rho_P(r) = A_c g^{(3)}(\hat{\alpha}_c, r) + A_v g^{(3)}(\hat{\alpha}_v, r) \quad (18)$$

with range parameters

$$\begin{aligned} \hat{\alpha}_v^2 &= \alpha_v^2 + \left(\frac{A_c \alpha}{A_v + A_c} \right)^2, \\ \hat{\alpha}_c^2 &= \alpha_c^2 + \left(\frac{A_v \alpha}{A_v + A_c} \right)^2. \end{aligned} \quad (19)$$

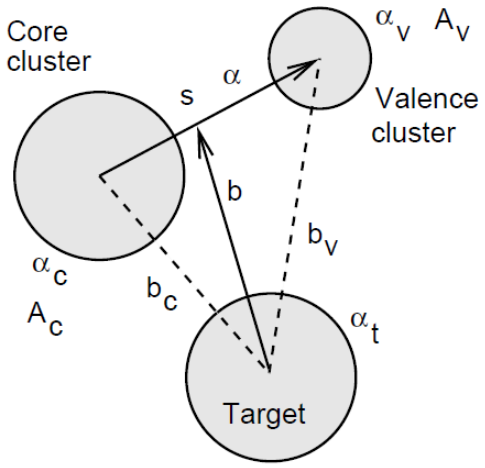

Fig.1: the two-cluster projectile and target coordinates.

The mean squared radius of the composite projectile $< r^2 >_P$ satisfies

$$A_P < r^2 >_P = A_c < r^2 >_c + A_v < r^2 >_v + \frac{A_v A_c}{A_P} < r^2 >= \frac{3}{2}\left(A_v \hat{\alpha}_v^2 + A_c \hat{\alpha}_c^2\right) \quad (20)$$

This approach provides a projectile density with distinct components due to the valence and core clusters. Such simple two component forms can be employed for calculating the density distributions of light exotic nuclei and also employed as input to optical limit calculations of reaction cross sections. However, a particular projectile single particle density, described by a given (A_c, A_v) mass split and choice of the two component ranges $(\hat{\alpha}_c, \hat{\alpha}_v)$, does not define the underling structure of the projectile. If one of the original clusters is pointlike, for example $\alpha_v = 0$, then fixing $\hat{\alpha}_v$ and $\hat{\alpha}_c$ uniquely determines α and hence α_c.

3. Glauber model calculations of reaction cross sections

In the Glauber model [33], the internal motions of the particles within the projectile (P) and target (T) are assumed slow compared to the relative motion of the centers of mass of the projectile and target. The reaction cross section for a projectile incident upon a target is given by [34]

$$\sigma_R = 2\pi \int_0^\infty b[1 - T(b)]db\left(1 - \frac{B_c}{E_{cm}}\right), \quad (21)$$

where B_c is Coulomb barrier, E_{cm} is the kinetic energy in the center of mass system and $T(b)$ is the transparency function at impact parameter b. A straightforward calculation of $T(b)$ is very complicated. One of the simplest methods to calculate $T(b)$ is the Optical limit (OL) approximation. In this approximation, which ignores any correlations between particles in the projectile or target, $T(b)$ is written as the squared modulus of the elastic $S-$matrix for the projectile-target system [35]

$$T(b) = \left|S_{el}^{OL}(b)\right|^2, \quad (22)$$

where

$$S_{el}^{OL}(b) = \exp\left[iO_{PT}(b)\right], \quad (23)$$

and

$$O_{PT}(b) = \int_{-\infty}^{\infty} dR_3 \int d\vec{r}_1 \int d\vec{r}_2 \rho_P(r_1)\rho_T(r_2) f_{NN}\left(\left|\vec{R} + \vec{r}_1 - \vec{r}_2\right|\right) \quad (24)$$

is the overlap of the projectile and target ground state densities (ρ_P and ρ_T, respectively) with an effective nucleon-nucleon (NN) amplitude $[f_{NN}(r)]$ integrated along the assumed straight line path of the projectile's center of mass at impact parameter b. For zero-range NN amplitude and isospin $T = 0$ target, $f_{NN}(r)$ has the form [35]

$$f_{NN}(r) = (i\bar{\sigma}_{NN}/2)\delta(r) \quad (25)$$

where $\bar{\sigma}_{NN}$ is the average of the free neutron-neutron (nn) and neutron-proton (np) total cross section at the energy of interest and given as [36]

$$\bar{\sigma}_{NN} = \frac{N_P N_T \sigma_{nn} + Z_P Z_T \sigma_{pp} + N_P Z_T \sigma_{np} + N_T Z_P \sigma_{np}}{A_P A_T} \quad (26)$$

where:

N_P, N_T : are the neutron number of projectile and target, respectively.

Z_P, Z_T: are the proton number of projectile and target, respectively.

A_P, A_T: are the mass number of projectile and target, respectively.

The nucleon- nucleon cross sections (σ_{pp}, σ_{nn} *and* σ_{np}) are given by Charagi formula [36]

$$\sigma_{pp} = \sigma_{nn} = 13.73 - \frac{15.04}{\beta} + \frac{8.76}{\beta^2} + 68.67\beta^4$$
$$\sigma_{np} = -70.67 - \frac{18.18}{\beta} + \frac{25.26}{\beta^2} + 113.85\beta \quad (27)$$

where σ_{pp}, σ_{nn} and σ_{np} are expressed in mb and $\beta = v/c$.

Expressing the projectile-target separation in cylindrical coordinates $\vec{R} = (\vec{b}, R_3)$, where $z = 3$ is the axis chosen along the incident beam direction, then [with the help of Eqs. (24) and (25)] Eq. (23) gives

$$S_{el}^{OL}(b) = \exp\left[-\frac{\bar{\sigma}_{NN}}{2}\int d\vec{r}_1 \int d\vec{r}_2 \rho_P^z(r_1)\rho_T^z(r_2)\delta(\left|\vec{b} + \vec{r}_1 - \vec{r}_2\right|)\right]. \quad (28)$$

Integrating over the coordinates r_2 then replacing r_1 by s, we obtain

$$S_{el}^{OL}(b) = \exp\left[-\frac{\bar{\sigma}_{NN}}{2}\int d\vec{s}\rho_P^z(s)\rho_T^z(\left|\vec{b} + \vec{s}\right|)\right], \quad (29)$$

where $\rho_{P(T)}^z(s)$ is the z-direction integrated nucleon density distribution expressed as

$$\rho_{P(T)}^z(s) = \int_{-\infty}^{\infty} \rho_{P(T)}\left(\sqrt{s^2 + z^2}\right)dz. \quad (30)$$

It is obvious from Eq. (29) that the calculations of $S_{el}^{OL}(b)$ requires only the projectile and target ground state densities. For simplicity, both densities are described by single Gaussian functions with range parameters α_P and α_T, respectively.

Results and discussion

The ground state proton, neutron and matter densities of exotic one-neutron halo nuclei ^{11}Be ($S_n = 504$keV, $T_{1/2} = 13.81$ s) [37, 38] and ^{15}C ($S_n = 1218$keV, $T_{1/2} = 2.449$ s) [37, 38] are studied by means of the TFSM [31, 32] and BCM [33].

In TFSM, the calculations are based on using different model spaces for the core and the valence (halo) neutron. The single particle harmonic oscillator wave functions are employed with two different size parameters β_c [for core nuclei ^{10}Be ($J^\pi, T = 0^+, 1$) and ^{14}C ($J^\pi, T = 0^+, 1$)] and β_v (for the halo neutron). The valence (halo) neutron in ^{11}Be ($J^\pi, T = 1/2^-, 3/2$) is assumed to be in a pure $1p_{1/2}$ while that in ^{15}C ($J^\pi, T = 1/2^+, 3/2$) is considered as admixture between two configurations $[^{14}C(0^+) \otimes \nu_{2s_{1/2}}]_{J=1/2^+}$ and $[^{14}C(2^+) \otimes \nu_{1d_{5/2}}]_{J=1/2^+}$, where $\nu_{2s_{1/2}}$ and $\nu_{1d_{5/2}}$ refer to the halo neutron wave functions of $2s_{1/2}$ and $1d_{5/2}$. The matter density distribution of the halo nucleus ^{15}C is obtained by adding the density of the core to that of the valence (halo) neutron. For simplicity, the density distributions of the ground ($J^\pi, T = 0^+, 1$) and excited ($J^\pi, T = 2^+, 1$) states of ^{14}C are supposed to be the same. The configurations $(1s_{1/2})^4$, $(1p_{3/2})^6$ and $(1s_{1/2})^4$, $(1p_{3/2}, 1p_{1/2})^{10}$ are assumed for core nuclei ^{10}Be and ^{14}C, respectively. For ^{14}C core, the ground state average occupation numbers $1p_{3/2}$=7.718 and $1p_{1/2}$=2.282, in mixed $(1p_{3/2}, 1p_{1/2})^{10}$, are obtained by performing shell model calculations using OXBASH code [39] with realistical Cohen-Kurath interaction CKI [40]. Values of $\beta_c = 1.574$ fm and 1.55 fm are preferred for core nuclei ^{10}Be and ^{14}C, which provide matter rms radii to these core nuclei equal to 2.28 fm (for ^{10}Be) and 2.3 fm (for ^{14}C), which are in astonishing agreement with the observed rms radii 2.28 ± 0.02 fm [41] (for ^{10}Be) and 2.3 ± 0.07 fm [42] (for ^{14}C). To reproduce

the observed matter rms radii of ^{11}Be (2.73 ± 0.05 fm [42]) and ^{15}C (2.783 ± 0.092 fm [42]), values of $\beta_v = 3.498$ and 3.455 fm are selected for ^{11}Be and ^{15}C, respectively. The above values of β_v and β_c provide results for matter rms radii equal to 2.73 fm (for ^{11}Be) and 2.783 fm (for ^{15}C), which are in excellent agreement with those of observed values.

In BCM [33], the halo nucleus is considered as a composite projectile consisting of core and valence clusters bounded in a state of relative motion [Fig.1]. The internal densities of the clusters, given by Eq. (16), are described by single particle Gaussian wave functions. The composite projectile densities of ^{11}Be and ^{15}C are calculated by Eq. (18).

Figure 2 shows the calculated matter density distributions (solid lines) obtained via TFSM [Figs. 2(a) and 2(c)] and BCM [Figs. 2(b) and 2(d)]. The top and bottom panels correspond to halo nuclei ^{11}Be and ^{15}C, respectively. The contributions of the core (dashed lines) and the halo neutron (dash-dotted lines) to the matter densities are also shown in these figures. The experimental matter densities of ^{11}Be [43] and ^{15}C [19] are displayed by shaded areas, for comparison. The solid lines in Figs. 2(a) and 2(b), which correspond to the halo nucleus ^{11}Be, agree well with the experimental data and show almost the same degree of accordance with the data. The solid lines in Fig. 2(c) (calculated by considering mixing configurations with occupation probabilities of 0.55 in $2s_{1/2}$ and 0.45 in $1d_{5/2}$ for the halo neutron) and 2(d) agree reasonably the experimental data. Moreover, the solid line in Fig. 2(d) is better describing the data than that in Fig. 2(c). The long tail behavior (which is a distinctive feature of halo nuclei) is revealed in all solid lines of Figs. 2(a), 2(b), 2(c) and 2(d), which is in agreement with the experimental data.

Fig. 3 demonstrates the results as in Fig. 2 but for the calculated proton and neutron density distributions displayed as dashed and dash-dotted lines, respectively. The long tail performance is clearly noticed in the dash-dotted lines. This performance is associated to the existence of the outer neutron in the halo orbits. The steep slope performance is obviously observed in the dashed lines due to the absence of protons in the halo orbit, where all protons of these nuclei are found in its core only. The difference between the calculated neutron and proton rms radii is $R_n - R_p = 2.99 - 2.22 = 0.77$ fm for ^{11}Be and $R_n - R_p = 3.07 - 2.28 = 0.79$ fm for ^{15}C. This difference gives an supplementary support for the halo structure of these nuclei.

Fig. 4 exhibits the comparison between the calculated matter density distribution of the halo nucleus ^{11}Be (^{15}C) (displayed as solid line) and that of a stable nucleus ^{9}Be (^{12}C) (displayed as dashed line). The size parameter of the harmonic oscillator radial wave function $\beta = 1.661$ fm ($\beta = 1.572$ fm) is utilized for a stable nucleus ^{9}Be (^{12}C) to reproduce the observed matter rms radius 2.38 fm (2.31 fm) of this nucleus. The calculated densities in Figs. 4(a) and 4(c) [obtained via TFSM] are compared with corresponding densities in Figs. 4(b) and 4(d) [obtained via BCM]. It is clear from these figures that the solid and dashed lines are diverse. As the outer neutron in ^{11}Be (^{15}C) is weakly bound, the solid line has a longer tail than that of the dashed line. Figures 2 and 3 provide the conclusion that the halo phenomenon in ^{11}Be and ^{15}C is connected to the outer neutron but not to the core nucleons.

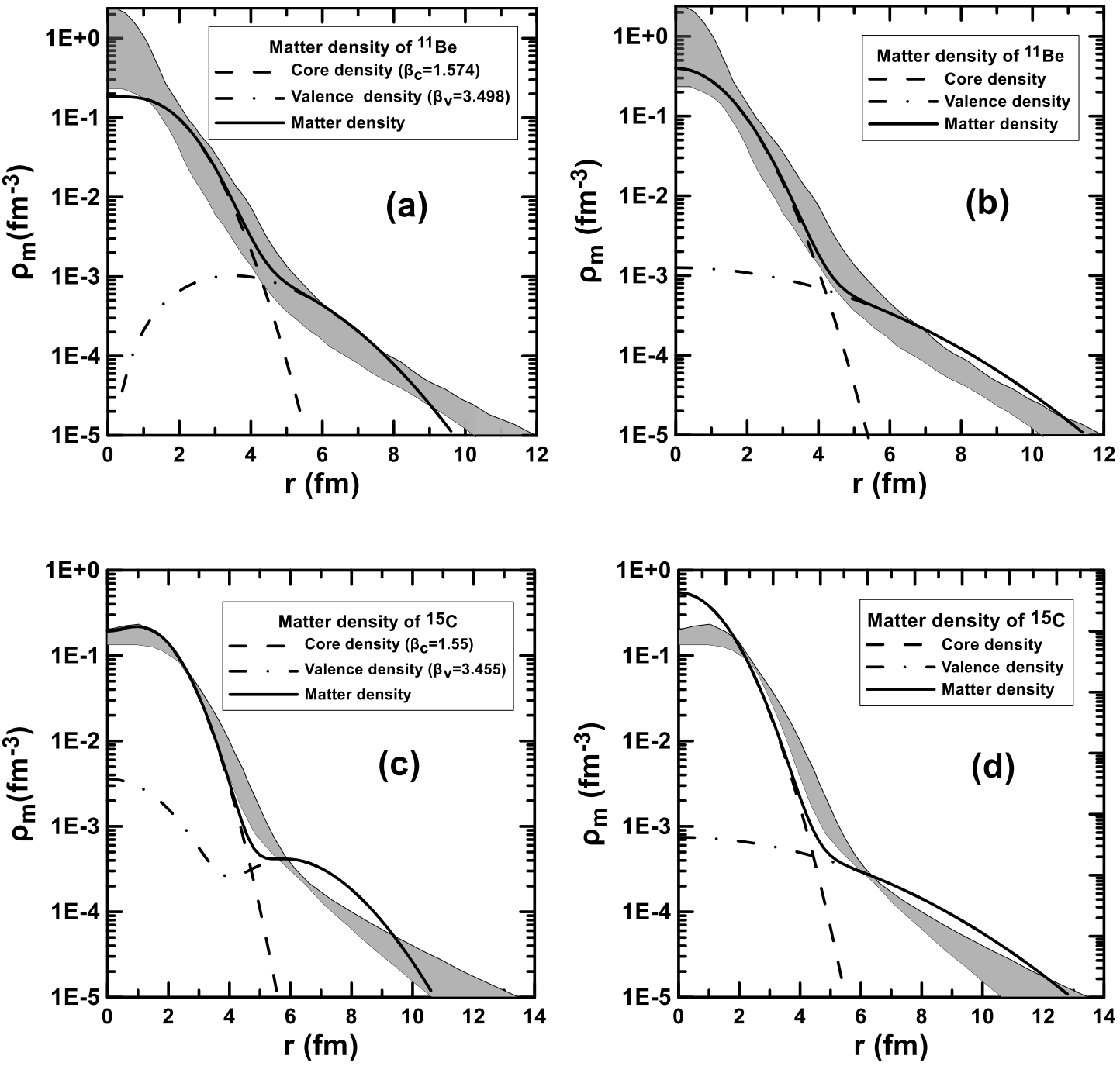

Fig.2: The calculated matter density distributions obtained via TFSM [Figs. (a) and (c)] and BCM [Figs. (b) and (d)]. The top and bottom panels correspond to halo nuclei ^{11}Be and ^{15}C, respectively. The shaded area shows the experimental matter density distribution of ^{11}Be [43] and ^{15}C [19].

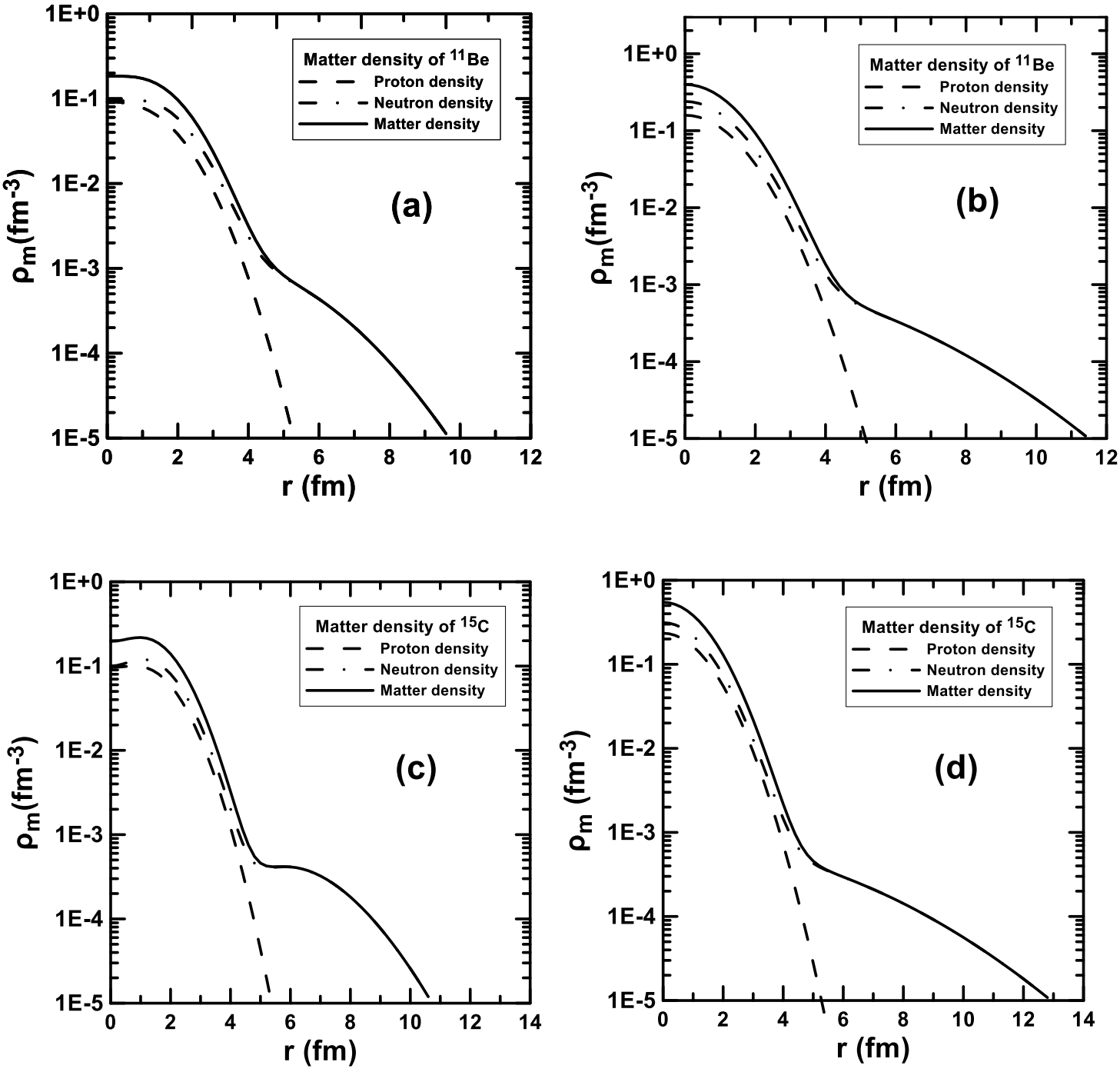

Fig.3: Neutron, proton and matter density distributions obtained via TFSM [Figs. (a) and (c)] and BCM [Figs. (b) and (d)]. The top and bottom panels correspond to halo nuclei ^{11}Be ***and*** ^{15}C***, respectively.***

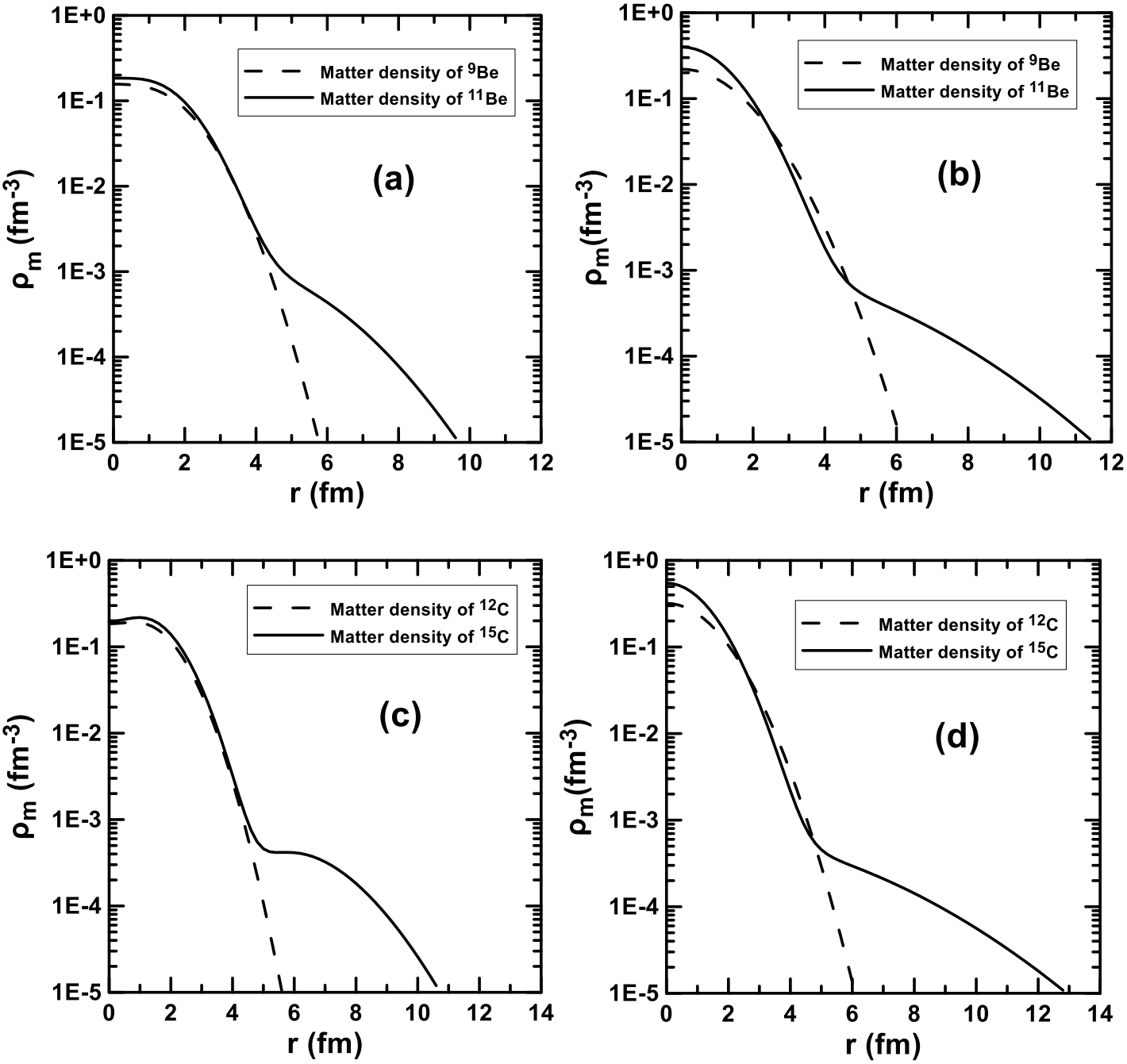

Fig.4: The comparison between the calculated matter density of unstable and stable nuclei. The left and right columns correspond to the calculations of TFSM and BCM, respectively. The top and bottom panels correspond to (^{9}Be, ^{11}Be) and (^{12}C, ^{15}C), respectively.

Elastic electron scattering proton form factors, which are simply given as Fourier transform of the ground state proton density distributions, for these halo nuclei are also calculated via the plane wave born approximation (PWBA). As the calculations in the BCM do not distinguish between protons and neutrons, the calculations of the proton form factors are restricted only by the TFSM.

Fig. 5 illustrates the comparison between the calculated C_0 elastic proton form factors of halo nuclei (solid lines) and those of stable nuclei (dashed lines). The calculated proton form factors in Figs. 5(a) and 5(b) correspond to (^{11}Be, ^{9}Be) and (^{15}C, ^{12}C) nuclei, respectively. The proton form factor is independent on detailed properties of the neutron halo. The major difference between the calculated form factor of the halo nucleus ^{11}Be (^{15}C) and that of a stable nucleus ^{9}Be (^{12}C) is the difference in the center of mass correction which depends on the mass number and the size parameter β which is assumed in this case equal to the average of β_c and β_v In Fig. 5(a) [Fig. 5(b)], each of the solid line and the dashed line has one diffraction minimum located at momentum transfer $q = 2.096$ fm^{-1} for ^{9}Be and at $q = 2.215$ fm^{-1} for ^{11}Be [$q = 1.940$ fm^{-1} for ^{12}C and at $q = 1.962$ fm^{-1} for ^{15}C] and one diffraction maximum located at $q = 2.423$ fm^{-1} for ^{9}Be and at $q = 2.587$ fm^{-1} for ^{11}Be [$q = 2.251$ fm^{-1} for ^{12}C and at $q = 2.340$ fm^{-1} for ^{15}C]. The location of the minimum of the halo ^{11}Be (^{15}C) has forward shift as compared with the minimum of a stable ^{9}Be (^{12}C).

The reaction cross sections (σ_R) are studied by means of the Glauber model with an optical limit approximation at high energies for (^{11}Be and ^{15}C) projectiles incident on the ^{12}C (rms radius= 2.31 ± 0.02 [42]) target using the ground state densities of these nuclei. The densities of the projectile and target are described by single Gaussian functions with range parameters α_P and α_T for projectile and target nuclei, respectively. The calculated reaction cross sections are listed in table 1 along with the corresponding experimental data taken from [42]. The calculated σ_R at 790 MeV for ^{11}Be+^{12}C system is 946 mb, which agrees well with the corresponding experimental data 942 ± 8 mb [42] within quoted error. The calculated σ_R at 730 MeV for ^{15}C+^{12}C system is 1022 mb, which agrees reasonably with the analogous measured data 945 ± 10 mb [42].

Table 1: Calculated reaction cross sections for ^{11}Be and ^{15}C exotic nuclei.

Exotic Nuclei	Experimental rms radii (fm)	Calculated σ_R (mb)	Experimental σ_R (mb)	Energy (MeV)
^{11}Be	2.73±0.05 [42]	946	942±8 [42]	790
^{15}C	2.783±0.092 [42]	1022	945±10 [42]	730

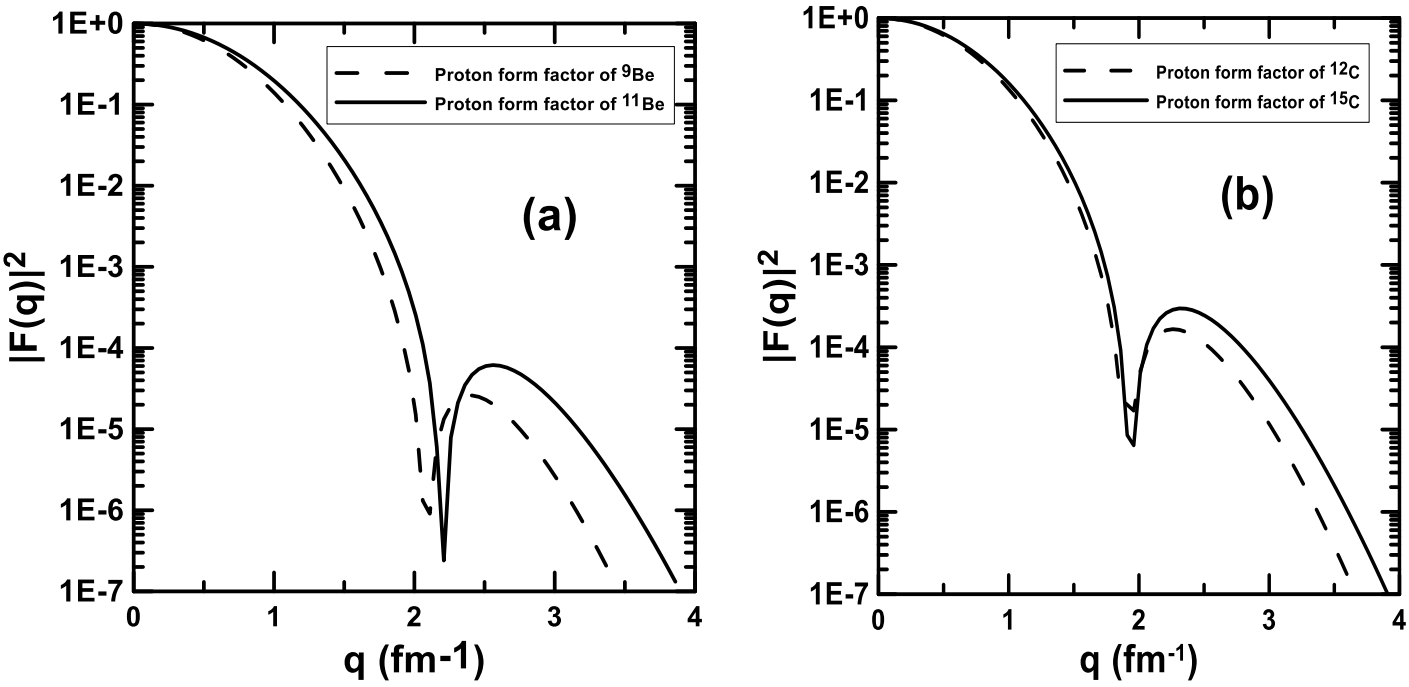

Fig.5: The comparison between the calculated proton form factors of unstable (exotic) nuclei (^{11}Be, ^{15}C) and those of stable nuclei (^{9}Be, ^{12}C).

Conclusions

The ground state proton, neutron and matter densities of exotic one-neutron halo nuclei ^{11}Be and ^{15}C are studied by means of the TFSM and BCM. The long tail performance, presumed as a typical property for the halo structure, is clearly revealed in the calculated neutron and matter density distributions of these exotic nuclei. Moreover, the noticeable difference which is found between the calculated overall neutron and proton rms radii as well provides a supplementary support for the halo structure of these nuclei.

Elastic electron scattering proton form factors for these exotic halo nuclei are also studied using the TFSM. It is found that the major difference between the calculated form factor of unstable exotic nucleus ^{11}Be (^{15}C) and that of a stable nucleus ^{9}Be (^{12}C) is the difference in the center of mass correction which depends on the mass number and the size parameter β, which is assumed in this case equal to the average of β_c and β_v.

The reaction cross sections for these exotic nuclei are studied by means of the Glauber model with an optical limit approximation using the ground state densities of the projectile and target, where these densities are described by single Gaussian functions. The calculated reaction cross sections at high energy are in agreement with the measured data.

The analysis of the present study suggests that the structure of the halo neutron for ^{11}Be is a pure $1p_{1/2}$ configuration while that for ^{15}C is mixed configurations with dominant ($2s_{1/2}$).

References

[1] I. Tanihata, H. Hamagaki, O. Hashimoto, Y.Shida, N. Yoshikawa, K. Sugimoto, O.Yamakawa, T. Kobayashi, and N. Takahashi, Phys. Rev. Lett., 55 (1985) 2676.

[2] P. G. Hansen and B. Jonson, Europhys. Lett., 4 (1987) 409.
[3] W. Zaijun, R. Zhongzhou, Science in China Series G Physics and Astronomy,47 (2004) 42.
[4] B. Blank , C. Marchand , M.S. Pravikoff, T. Baumann, F. Bou, H. Geissel, M. Hellström, N. Iwasa, W. Schwab, K. Sammerer and M. Gai, Nuclear Physics A, 624 (1997) 242.
[5] H.Y. Zhang, W.Q. Shen, Z.Z. Ren, Y.G. Ma, W.Z. Jiang, Z.Y. Zhu, X.Z. Cai, D.Q. Fang, C. Zhong, L.P. Yu, Y.B.Wei, W.L. Zhan, Z.Y. Guo, G.Q. Xiao, J.S. Wang, J.C. Wang, Q.J. Wang, J.X. Li, M. Wang and Z.Q. Chen, Nucl. Phys., A 707 (2002) 303.
[6] Anis Dadi, Ph.D. Thesis, University of Heidelberg, Germany (2012).
[7] G.Wen-Jun, J. Huan-Qing L. Jian-Ye, Z.,REN Zhong-Zhou, and L. Xi-Guo, Commun, Theor. Phys., 40 (2003) 577.
[8] H. ZhengGuo, W. Meng, X. HuShan, S. ZhiYu, W. JianSong, X. GuoQing, Z. WenLong, X. ZhiGang, M. RuiShi, L. Chen, Z. XueYing, Z. HongBin, Z. TieCheng, X. ZhiGuo, W. Yue, C. RuoFu, H. TianHeng, F. Fen, G. Qi, H. JianLong, Z.HANG XueHeng, Z. Chuan, Y. YuHong and G. ZhongYan, Science in China Series G: Physics, Mechanics and Astronomy, 51 (2008) 781.
[9] J. S. Vagen, D. K. Gridne, H. Heiberg-Andersen, B. V. Danilin, S. N. Ershov, V. I. Zagrebaev, I. J. Thompson, M. V. Zhukov and J. M. Bang. Phys. Scr., T88 (2000) 209.
[10] M. V. Zhukov, B.V. Danilin, DV. Fedorov, J.M. Bang, I.J. Thompson and J.S. Vaagen, Phys. Rep., 231 (1993) 151.
[11] A. N. Antonov, D. N. Kadrev, M. K. Gaidarov, E. Moya de Guerra, P. Sarriguren, J. M. Udias, V. K. Lukyanov, E. V. Zemlyanaya, G. Z. Krumova Phys. Rev., C 72 (2005) 044307.
[12] Technical Proposal for the Design, Construction, Commissioning, and Operation of the ELISe setup, Haik Simon, GSI Internal Report, Dec. 2005.
[13] T. Suda, K. Maruyama, Proposal for the RIKEN beam factory, RIKEN, 2001; M. Wakasugi, T. Suda, Y. Yano, Nucl. Inst. Meth. Phys., A532 (2004) 216.
[14] A. Bhagwat, Y.K. Gambhir, and S.H. Patil, Eur. Phys. J., A 8, (2000) 511.
[15] J.S. Al-Khalili, Eur. Phys., J. A 15 (2002) 115.
[16] Z.Y. Zhu, W.Q. Shen, Y.H. Cai, Y. G. Ma, Phys. Lett., B 328 (1994) 1.
[17] A. Ozawa Eur. Phys. J., A 13 (2002) 163.
[18] L. Zu-Hua, Chin. Phys. Lett., 19, 8 (2002) 1071.
[19] D. Q. Fang, T. Yamaguchi, T. Zheng A. Ozawa, M. Chiba, R. Kanungo, T. Kato, K. Morimoto, T. Ohnishi, T. Suda, Y. Yamaguchi, A. Yoshida, K. Yoshida, and I. Tanihata, Phys. Rev., C 69 (2004) 034613.
[20] G.Y. Qing and R. Z. Zhou, Chin. Phys. Lett., 24 (2007) 652.
[21] C. Xiangzhou, F. Jun, S. Wenqing, M. Yugang, W. Jiansong, and Y. Wei, Phys. Rev., C 58 (1998) 572.
[22] I. Tanihata, D. Hirata, T. Kobayashi, S. Shimoura, K. Sugimoto, and H. Toki, Phys. Lett., B 289 (1992) 261.
[23] M.Tetsuaki , Ph.D.Thesis, University of Tsukuba (2011).
[24] Y. Ogawa, K . Yabanab and Y. Suzuki, Nucl. Phys., A 543 (1992)722.
[25] A. Ozawa, T. Baumann, L. Chulkov, D. Cortina, U. Datta, J. Fernandez, H. Geissel, F. K.Hammache, Itahashi, M. Ivanov, R. Janik, T. Kato, K. Kimura, T. Kobayashi, K. Markenroth, M. Meister, G. Münzenberg, T. Ohtsubo, S. Ohya, T. Okuda, A.A. Ogloblin, V. Pribora, M. Sekiguchi, B. Sitár, P. Strmen, S. Sugimoto, K. Sümmerer, T. Suzuki, I. Tanihata and Y. Yamaguchi, Nucl. Phys., A 709 (2002) 60.
[26] Z. Yao-Lin, M. Zhong-Yu and C. Bao-Qiu, Commun. Theor. Phys., 36 (2001) 313.
[27] I. Tanihata, J. Phys., G 22 (1996) 157.

[28] Y.L. Zhao, Z.Y. Ma, B.Q. Chen and X.Q. Sun, High Energy Phys. Nucl. Phys., 6 (2001) 506.
[29] B. A. Brown, R. Radhi, and B. H. Wildenthal, Phys. Rep., 101 (1983) 313.
[30] Brown B. A., Etchegoyen A., Godwin N. S., Rae W. D. M., Richter W. A., Ormand W.E., Warburton E. K., Winfield J. S., Zhao L., Zimmerman C. H. 2005. Oxbash for Windows PC. MSU-NSCL report number1289.
[31] T. T. S. Kuo, H. Muether, and K. Amir-Azimi-Nili, Nucl. Phys., A 606 (1996) 15.
[32] T. T. S. Kuo, F. Krmpotic, and Y. Tzeng, Phys. Rev. Lett., 78 (1997) 2708.
[33] J. A. Tostevin, R. C. Johnson and J. S. Al-Khalili, Nucl. Phys., A 630 (1998) 340c.
[34] T. Zheng, T. Yamaguchi, A. Ozawa, M. Chiba, R. Kanungo, T. Kato, K. Katori, K. Morimoto, T. Ohnishi, T. Suda, I. Tanihata, Y. Yamaguchi, A. Yoshida, K. Yoshida, H. Toki and N. Nakajima, Nucl. Phys., A 709 (2002) 103.
[35] J. A. Tostevin and J. S. Al-Khalili, Nucl. Phys., A 616 (1997) 418c.
[36] S.K. Charagi and S.K. Gupta, Phys. Rev. C 41 (1990) 1610.
[37] G. Audi and A. H.Wapstra, Nucl. Phys., A565 (1993) 66.
[38] G. Audi, O. Bersillon, J. Blachot and A.H. Wapstra, Nucl. Phys., A 729 (2003) 3.
[39] B. A. Brown, A. Etchegoyen , N. S. Godwin, W. D. M. Rae, W. A. Richter, W.E. Ormand, E. K. Warburton, J. S. Winfield, L. Zhao, C. H. Zimmerman, 2005. Oxbash for Windows PC. MSU-NSCL report number1289.
[40] S. Cohen and D. Kurath, Nucl. Phys., 73 (1965) 1.
[41] I. Tanihata, T. Kobayashi, O. Yamakawa, S. Shimoura, K. Ekuni, K. Sugimoto, N. Takahashi, T. Shimoda and H. Sato, Phys., Lett. B 206 (1988) 592.
[42] A. Ozawa, T. Suzuki and I. Tanihata, Nucl. Phys., A 693 (2001) 32.
[43] M. Fukuda, T. Ichihara, N. Inabe, T. Kubo, H. Kumagai, T. Nakagawa, Y. Yano, I. Tanihata, M. Adachi, K. Asahi, M. Kouguchi, M. Ishihara, H. Sagawa and S. Shimoura, Phys. Lett., B 268 (1991) 339.